LANGMUIR

pubs.acs.org/Langmuir Article

Correlation between Electrostatic and Hydration Forces on Silica and Gibbsite Surfaces: An Atomic Force Microscopy Study

Aram Klaassen, Fei Liu, Frieder Mugele, and Igor Siretanu*

Cite This: *Langmuir* 2022, 38, 914−926 Read Online

ACCESS | Metrics & More | Article Recommendations | Supporting Information

ABSTRACT: The balance between hydration and Derjaguin−Landau−Verwey−Overbeek (DLVO) forces at solid−liquid interfaces controls many processes, such as colloidal stability, wetting, electrochemistry, biomolecular self-assembly, and ion adsorption. Yet, the origin of molecular scale hydration forces and their relation to the surface charge density that controls the continuum scale electrostatic forces is poorly understood. We argue that these two types of forces are largely independent of each other. To support this hypothesis, we performed atomic force microscopy experiments using intermediate-sized tips that enable the simultaneous detection of DLVO and molecular scale oscillatory hydration forces at the interface between composite gibbsite:silica−aqueous electrolyte interfaces. We extract surface charge densities from forces measured at tip−sample separations of 1.5 nm and beyond using DLVO theory in combination with charge regulation boundary conditions for various pH values and salt concentrations. We simultaneously observe both colloidal scale DLVO forces and oscillatory hydration forces for an individual crystalline gibbsite particle and the underlying amorphous silica substrate for all fluid compositions investigated. While the diffuse layer charge varies with pH as expected, the oscillatory hydration forces are found to be largely independent of pH and salt concentration, supporting our hypothesis that both forces indeed have a very different origin. Oscillatory hydration forces are found to be distinctly more pronounced on gibbsite than on silica. We rationalize this observation based on the distribution of hydroxyl groups available for H bonding on the two distinct surfaces.

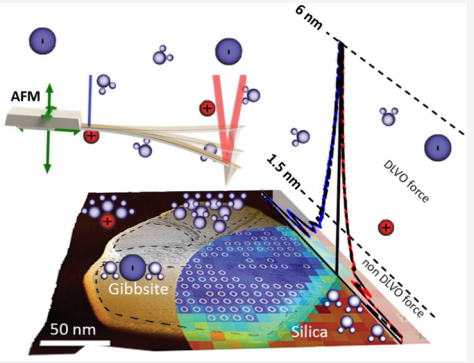

1. INTRODUCTION

The forces between charged surfaces, colloidal particles, dissolved ions, and organic molecules in ambient aqueous electrolyte are essential in diverse scientific disciplines, like colloid science,[1] biophysics,[2] (electro/photo)catalysis,[3] and environmental geochemistry.[4] They control colloidal stability, dynamics, self-assembly,[5−7] ion adsorption,[8] friction,[9] adhesion,[10] and many other properties. For not too high salt concentrations, these forces are well described on the colloidal scale by the classical Derjaguin−Landau−Verwey−Overbeek (DLVO) theory of colloid science that combines electric double-layer (EDL) forces with a characteristic range set by the Debye screening length and van der Waals interaction.[1,11] Yet, it was already pointed out by Langmuir that this picture is incomplete and that the ultimate formation of contact between two solutes should be governed by short-range forces related to the molecular structure of the solvent, i.e., by hydration forces in the case of aqueous solutions.[1,11−16]

Recent advances in both simulations and experiments have revealed many important details regarding the variations in the structure and dynamics of interfacial water within the first nanometer or so from a solid surface.[17−22] However, different techniques probe distinct aspects of the interfacial water, and a consistent and comprehensive picture has yet to emerge. For instance, X-ray reflectivity, scattering, and X-ray surface diffraction provide detailed information regarding the distribution of the electron density at solid−electrolyte interfaces that provides information about the positions of the ions and water molecules, revealing adsorption sites and configurations (inner shell vs outer shell) with unparalleled accuracy.[23−26] These microscopic structures are governed by coordination effects and interactions with the immediate local environment. As a consequence, the corresponding modulations of the interfacial water structure are typically limited to a very short range of no more than ∼1 nm, as supported by a large number of molecular simulations.[20,27,28] On the other hand, nonlinear optical spectroscopies[18,29−31] have revealed average orientations of water molecules in the vicinity of the interface and provided exquisite correlations between these orientations and measured colloidal scale surface potentials. These experiments and simulations reveal a much longer range of the perturbation of the water structure up to the Debye screening length from the interface, i.e., up to the colloidal scale.[18,29−31]

Received: August 4, 2021
Revised: December 29, 2021
Published: January 13, 2022

https://doi.org/10.1021/acs.langmuir.1c02077
Langmuir 2022, 38, 914−926

While X-rays and nonlinear optical spectroscopies probe complementary (positional vs orientational) aspects of interfacial water, neither of them provides direct access to the forces that drive interfacial assembly and the other processes mentioned above. Interfacial force measurements using the surface forces apparatus (SFA)[32−36] and atomic force microscopy (AFM) have revealed detailed information about DLVO and non-DLVO forces such as hydration. In contrast to the SFA, AFM provides more flexibility regarding the choice of surface materials and allows for the simultaneous in situ observation of different (heterogeneous) materials under identical conditions within subnanometer spatial resolution.

AFM measurements also allow one to shift the relative importance of different contributions to the total force by varying the tip size. Colloidal probe force microscopy[22,37−42] and AFM[43−46] with blunted tips with a radius of a few tens of nanometers have enabled detailed studies of DLVO forces and provided new insights, in particular, on ions adsorption, charge regulation, and ion correlations as well as the role of surface defects and heterogeneities. Experiments with "supersharp" tips (radius ≈ 1−2 nm), on the other hand, have revealed detailed correlations between hydration forces and the local bonding environment for water and/or adsorbed ions on the lattice of typically crystalline surfaces, often complemented by numerical simulations.[17,28,47−52] Yet, while colloidal probe measurements are, in general, unable to resolve effects arising from the discreteness of ions and water molecules, the molecular scale force measurements are in turn not sensitive to the classical colloidal scale DLVO forces. This mutual exclusiveness hampers systematic investigations of the dependence of these forces on the fluid composition and could only be overcome by carrying out separate experiments with supersharp molecular scale and blunt colloidal scale probes on the same type of sample.[43]

The purpose of the present work is to bridge the gap between colloidal scale continuum DLVO forces and molecular scale hydration forces. To this end, we perform two three-dimensional force−volume mapping experiments on heterogeneous surfaces consisting of crystalline gibbsite nanoparticles adsorbed on an amorphous silica substrate in ambient aqueous sodium chloride (NaCl) solutions of variable concentration and pH. Both materials serve as an excellent model system for fundamental studies of complex electrolyte/oxide interfaces and are often used in many industrial processes and various chemical, medical, and geological applications. Gibbsite is a good model for some clay mineral surfaces and an important phase in the aluminum production industry. Gibbsite was chosen because it can be synthesized reproducibly to yield suspensions of essentially monodispersed particles and less heterogeneity as compared to natural clay particles. The hydration structure of silica and gibbsite is related to the physicochemical properties, such as wetting, adsorption and retention of organic/inorganic species, reactivity, colloidal stability of particles, etc. Thus, measuring and understanding the silica−gibbsite system surface charge and hydration structure is of interest.

The experiments were performed using an intentionally slightly blunted AFM tip that allows for simultaneous mapping of both the continuum EDL forces and the short-range hydration forces. The hydration structure of the crystalline gibbsite nanoparticles is more pronounced than that on the amorphous silica surface, and the corresponding hydration forces hardly vary upon changing fluid composition, while the simultaneously measured continuum EDL forces reverse sign. We rationalize these results in terms of a microscopic picture of the hydration structure involving local binding geometries and the surface coverage with hydroxyl (OH) groups.

2. METHODS AND MATERIALS

2.1. Sample and AFM Probe Preparation. The gibbsite stock suspension (in 20 mM NaCl, pH 6) was provided by the research group of A. Philipse. The synthesis of the particles is described in a report by Wierenga et al.[53] Gibbsite [$Al(OH)_3$] mineral nanoparticles consist of stacked sheets of octahedral aluminum atoms coordinated by groups of 3 hydroxyl oxygen (O) atoms above and below the aluminum (Al) sheets. Gibbsite grows well along lateral (a and b) directions, resulting in thin hexagonally shaped nanoparticles.[80−82] These aluminum hydroxide sheets are similar to the octahedral sheets bonded to silicate sheets in clay minerals such as kaolinite, illite, and smectite.[4,83] Silicon substrate (Okmetic, 100 plane, P-type, 1 × 1 cm) with a 30 nm thickness, thermally grown at 1150 °C at low pressure in an O_2 atmosphere oxide layer, was used. The dissolution of the silica and gibbsite or the reprecipitation of new solid phases is negligible for the experimental observations here (at least within the time frame of the experiment, 24 h), as the solubility of the solid phases is low (dissolution rates up to 1×10^{-7} mol·m^{-2}·s^{-1}).[54,55]

The silica was cleaned in an ultrasonic bath for 15 min in a mixture of isopropanol, ethanol, and Millipore water (25/25/50% by volume) and subsequently rinsed with only Millipore water. Then, the substrate was air plasma cleaned (PDC-32G-2, Harrick Plasma, Ithaca, NY, USA) for 20 min. A 10 μL drop of diluted gibbsite suspension (gibbsite stock suspension diluted 100× in Millipore water) was placed on the cleaned silicon wafer. After a residence time of 60 s, in which the gibbsite particles settle on the substrate, the excess suspension was removed and the substrate was dried with a flow of nitrogen. Then, the sample was rinsed with Millipore water and dried. The surface coverage of gibbsite nanoparticles on silica substrate was less than 2−5%. The surface area to volume ratio for gibbsite was ∼0.05−0.1 m^2/L. The AFM cantilevers were cleaned using a mixture of isopropanol and ethanol (50/50%) and then plasma cleaned for 20 min. Sodium chloride (NaCl) (99% ACS reagent grade, Sigma-Aldrich) stock solutions were prepared by dissolving salt in Millipore water. The pH was adjusted by adding HCl (ACS reagent, 37%) or NaOH solutions (ACS reagent, ≥97.0%, pellets). All chemicals used were purchased from Sigma-Aldrich.

2.2. AFM Force Spectroscopy. Dynamic amplitude modulation (AM) imaging and force spectroscopy measurements[56] were performed with a commercial Asylum Research Cypher ES equipped with photothermal excitation.[57] First, in amplitude modulation (AM) imaging mode, the topography of the sample was taken. From this large image (Figure S1) a suitable gibbsite particle for force spectroscopy was chosen (dotted area in Figure S1). Then, force spectroscopy was achieved using the force volume map functionality in the Cypher MFP-3D software. In this mode, the mean deflection (u), amplitude (A), phase (φ), and drive frequency (ω) versus the measured piezo position (z_p) were recorded in a 2D grid over the area of interest. This results in a 3D volume of data of the tip sample approach and retraction curves. The tip−sample force gradient (interaction stiffness k_{int}) was calculated from the amplitude and phase shift vs distance curves using standard force inversion procedures as extensively described by Liu et al. and Klaassen et al.[45,56,57] We used silicon probes (MikroMash NSC36/Cr-Au BS) covered by a 1−2 nm thick native oxide layer and a golden backside coating on the cantilever. The cantilever parameters (spring constant k_c, quality factor Q, and eigenfrequency ω_0) were extracted from the thermal noise spectrum of the undriven cantilever in liquid at separation D = 20 nm, where the tip−sample interaction is negligible (see Figure S2). The values are $k_c \approx 2.5$ N/m, $\omega_0 \approx 49.8$ kHz, and $Q \approx 3.5$. To protect the shape of the tip apex, the amplitude signal was not allowed to drop below 80% of its free amplitude (∼1−2 nm). The experiments were performed in a liquid drop (0.2−0.4 mL) that entirely covered the sample (1 × 1 cm^2), sandwiched between the tip

https://doi.org/10.1021/acs.langmuir.1c02077
Langmuir 2022, 38, 914−926

holder and the sample. The sample was placed in a closed cell that allows for liquid exchange. The fluid was exchanged using two syringes by injecting a new solution while completely removing the old solution. The liquid exchange was done by replacing the drop volume (0.2−0.4 mL) at least 25 times. Before the next 3D force map was started, we ensured that the system was stabilized, which took approximately 5−10 min after a fluid exchange. The order of experiments was as follows: pH 6, 10 mM NaCl; pH 6, 100 mM NaCl; pH 9, 10 mM NaCl; pH 9, 100 mM NaCl; pH 4, 10 mM NaCl; pH 4, 100 mM NaCl; pH 6, 10 mM NaCl. Therefore, during a full cycle of experiment, the fluid exchange was done 7 times (each time 25× the total AFM cell fluid volume) plus excessive rinsing with MQ water in between. As shown in Figure S3, the forces (DLVO and hydration) on silica and gibbsite from the first and last experiments (in identical conditions pH 6, 10 mM NaCl) are nicely overlapping on top of each other. This indicates that the tip size and the surface properties of the tip and the sample (silica−gibbsite) did not change over the course of all experiments. All experiments presented here were carried out on the same gibbsite particles and at a constant temperature (29 ± 1 °C). During the extraction of the tip from the AFM probe holder for cleaning, the tip was damaged and it could not be imaged by scanning electron microscopy (SEM). In order to retrieve the tip radius, another approach had to be taken. From previous experiments with identical experimental settings, tip type, silica substrate, and conditions, we know the silica charge at pH 6 and 10 mM NaCl accurately. Therefore, from the data at pH 6 and 10 mM NaCl shown in Figure S3 we calculated the AFM tip radius by fitting the model electrostatic interactions to the experimental silica−silica force curves (tip radius as a fitting parameter). This results in a tip radius of ∼9 nm. Subsequently, the tip radius was fixed during the fitting procedure of the 3D force maps at pH 4, 6, and 9 with 10 and 100 mM NaCl and the surface charge maps of silica and gibbsite nanoparticle shown in Figure 4 were extracted.

2.3. Fitting Procedures and Surface Charge Determination. As extensively described earlier,[44,45] the measured force−distance curves were converted to surface charge using DLVO theory and the charge regulation model for the tip and silica−gibbsite sample.[58,59] To do so, we calculated the hypothetical force−distance curves for a given surface charge and regulation parameters and compare these curves with the measured curves using the surface charge and the equilibrium constants ($K_j = 10^{-pK_j}$) of the considered surface reactions as fitting parameters. To determine the force between the tip and the sample surface, we first calculated the disjoining pressure $\Pi(D)$ in the gap with height D between them. This pressure can be split into a contribution Π_{vdW} due to van der Waals interactions and an electrostatic double-layer contribution Π_{EDL}. The force on the tip was calculated by integrating Π over the spherical tip with radius R_{tip}

$$F_{int}(D) = \int_D^\infty k_{int}(D')\mathrm{d}D' = 2\pi R_{tip}\int_D^\infty [\Pi_{EDL}(D') + \Pi_{vdW}(D')]\mathrm{d}D' \quad (1)$$

Here, F_{int} is the interaction force, k_{int} is the interaction stiffness (force gradient), and D is the tip to surface distance.

The van der Waals contribution between an AFM probe with radius R and a flat surface was calculated using

$$\Pi_{vdW}(D) = -\frac{A_H}{6D^2} \quad (2)$$

where A_H is the Hamaker constant and D is the tip to surface distance. The Hamaker constants A_H were taken from the literature[60−62] and are fixed to 0.65×10^{-20} J for the (silica−water−silica) system and to 1.2×10^{-20} J for the (silica−water−gibbsite) system.

The electrostatic double-layer contribution contains the required information on the surface charge/potential. For a 1−1 electrolyte it is given by

$$\Pi_{EDL}(D) = 4c_\infty k_B T \sinh^2\left(\frac{e\psi}{2k_B T}\right) - \frac{\varepsilon\varepsilon_0}{2}\left(\frac{\partial\psi}{\partial z}\right)^2 \quad (3)$$

where c_∞ is the ion concentration in the bulk solution away from the substrates, k_B is the Boltzmann constant, T is the temperature, e is the elementary charge, and $\varepsilon\varepsilon_0$ is the dielectric permittivity of water. $\psi(z)$ is the electrostatic potential in the electrolyte at an arbitrary position $0 < z < D$ between the two solid surfaces. Calculation of the electric double-layer contribution requires knowledge of the potential $\psi(D)$ in the electrolyte. This potential is governed by the Poisson−Boltzmann (PB) equation

$$\frac{\partial^2}{\partial z^2}\left(\frac{e\psi}{k_B T}\right) = k^2 \sinh\left(\frac{e\psi}{k_B T}\right) \quad (4)$$

and the boundary conditions at both surfaces. k is the reciprocal of the Debye length

$$k = \sqrt{\frac{2e^2 c_\infty}{\varepsilon\varepsilon_0 k_B T}} \quad (5)$$

Here, we employ the charge regulation (CR) approximation. Due to surface reactions, the substrates acquire a charge density, σ_s, that depends on the concentration of the ions near the substrate and so on the local potential, ψ_s. This dependence is formally written as $\sigma_s = f_s(\psi_s, c_1^\infty, c_n^\infty, \Gamma, K_1, K_m)$, where Γ is the site density on the substrate and $K_j = 10^{-pK_j}$ are the equilibrium constants of the considered surface reactions. The surface reactions from which the surface charge−surface potential relations have been derived for silica and gibbsite have been explained in detail in a report by Zhao et al.[44] Here, we give only the final expression for the charge density $\sigma_S = f(\psi_s)$ for silica and gibbsite as obtained from the charge regulation model (Table S1). In the evaluation of σ_S (ψ_s) the site densities Γ of silica and gibbsite are set to 5 and 13.8 sites/nm^2, respectively.[44,61,63,64] The ion concentration and pH of the solution are also set as known values. Only the equilibrium constants K_j (K_{H1} and K_C for silica and K_{H2} and K_A for gibbsite) are used as free (fitting) parameters to optimize the agreement (using a least-squares fitting procedure) between the experimental data and the calculated model curves with a separation from 1.5 to 10 nm. The advantage of DLVO-CR is that the model force−distance curves that include the CR boundary condition describe the experimental data of a significantly wider range than the approximate solutions for constant potential (CP) and constant charge (CC) solutions.[44] As explained in a report by Zhao et al.,[44] this force analysis procedure results in accurate and reliable values for the diffuse layer charge densities on both surfaces, but the K_j values are not necessarily unique and depend on the assumed set of surface reactions. Therefore, we only report and discuss the surface charge density σ_S on the surfaces and not pK values. The DLVO interaction force between the tip and the surfaces is determined by integrating the pressure over the surface area of the tip with respect to the distance D. For the integration, we use the Derjaguin approximation for the sphere−flat plate geometry. Despite the small radius of the tip, for the fluid compositions investigated here (pH 4, 6, and 9 and 10 and 100 mM NaCl, i.e., at Debye lengths below 3 nm), the Derjaguin approximation is valid, as the Debye length is smaller compared to the tip−sample distance and the latter is smaller compared to the tip radius. This was also demonstrated in recent work by Todd and Eppell,[65−67] where the validity limits of the Derjaguin approximation with a sharp tip (7 nm) were investigated in detail. Note that the surface charge as determined from AFM (or SFA) force measurement is the diffuse layer charge, σ_d. This charge density is equal to the charge density resulting from (de)protonation of the surface hydroxyl groups of the substrate, σ_0, and from ion adsorption, σ_i, so $\sigma_d = -(\sigma_0 + \sigma_i)$, and is always lower than the charge density determined by a titration measurement that measures the total number of protons or ions adsorbing to or desorbing from a surface.[38,44]

2.4. Fitting Analysis of Force−Distance Curves and Extraction of Oscillatory Hydration Force. Using DLVO-CR theory, the force−distance curves can be accurately fitted only down to a separations of 1.5−2 nm (black dotted lines in Figure 2). To fit the total interaction stiffness (k_{TOT}) at separations smaller than 1.5 nm, where the continuum theories of the van der Waals force and

https://doi.org/10.1021/acs.langmuir.1c02077
Langmuir 2022, 38, 914−926

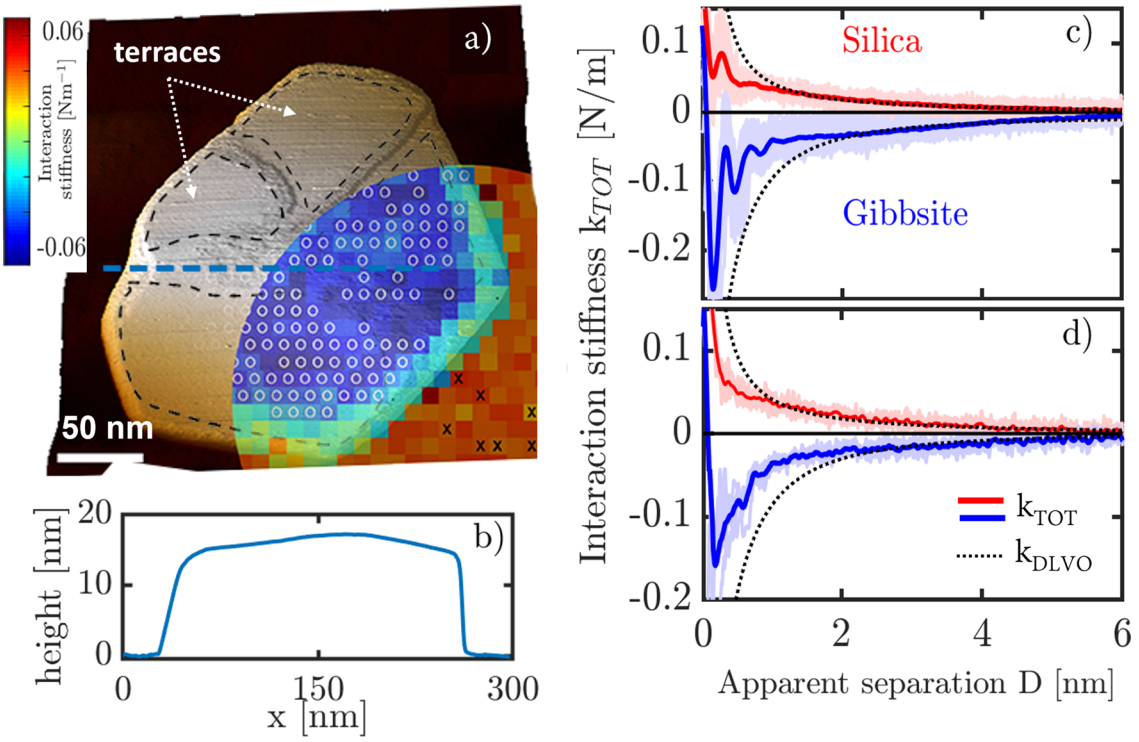

Figure 1. (a) Interaction stiffness map (at 2 nm from the surface) superimposed on an AM-AFM topography image of a gibbsite particle on silica substrate in a 10 mM NaCl pH 6 solution. Blue and green are approaches on gibbsite, which are negative; red is approaches on silica. Circles and crosses indicate the location of approaches with an oscillatory behavior. Examples are shown in c. Approaches without oscillatory behavior are shown in d. Shaded regions are the 10 individual approaches. Thick red and blue lines are their respective averages. Black dotted lines are DLVO interaction fits. Cross section of the particle is shown in b.

double-layer force (k_{EDL}) cannot describe the interactions (Figure 2),[43−45] we use a function (k_{int_TOT}) consisting of a superposition of a DLVO interaction (k_{DLVO} as described in the above section) and a short-range contribution k_{SR}. The short-range contribution is described by an empirical function consisting of a combination of a monotonically decaying exponential function ($k_{SR_{MON}}$) and a decaying oscillatory contribution ($k_{SR_{OSC}}$)[11,47,50] (eq 6). As the periodicity of the oscillations in $k_{SR_{OSC}}$ is very close to the size of the water molecule, we assign this force to a non-DLVO oscillatory hydration force $k_{HYD_{OSC}}$

$$k_{TOT}(D) = k_{DLVO} + k_{SR} = (k_{EDL} + k_{VDW}) + (k_{SR_{MON}} + k_{HYD_{OSC}}) = (k_{EDL} + k_{VDW}) + (A_{SR_{osc}}\cos(2\pi\sigma D - \varphi)e^{D/\lambda_{hyd_{osc}}} + A_{mon}De^{-D/\lambda_{mon}}) \quad (6)$$

where A_{EDL}, A_{osc}, and A_m are the magnitude of the electrical double-layer force, oscillatory (structural) hydration force, and monotonic short-range forces, φ is the phase shift, σ is the structural hydration layer spacing, and λ_{EDL}, λ_{osc}, and λ_m are the decay lengths of the electrical double-layer force, short-range oscillatory hydration force and short-range monotonic forces. A_H is the Hamaker constant, R is the radius of the sphere, and D is the tip to surface distance. This fitting step enabled us to quantify the strength (amplitude) and decay length of (i) the EDL force, (ii) the oscillatory hydration force, and (iii) the monotonically decaying short-range force as a function of fluid composition and lateral position on the sample. All of these fitting parameters are reported in Table S2.

2.5. Error Analysis. In this section, we discuss the influence of several parameters on the determination accuracy of the surface charge, the strength and decay length of the oscillatory hydration force, and the monotonically decaying short-range force. As already reported in our previous work,[45] the uncertainty in the absolute zero on the distance scale, geometry and size of the tip, limits of the fitting boundary, instrument sensitivity, thermal fluctuations, and others result in up to 20% error in the surface charge. The short-range forces, especially the monotonically decaying force, are affected by uncertainty in the above specified parameters and subtraction of DLVO forces. In particular, the accuracy of the tip area (tip radius) and the zero point determination (D = 0) strongly affect the absolute magnitude of the short-range monotonic force. Overall, we estimate the uncertainty of the tip radius to be up to ±2 nm. We fitted all parameters for the DLVO and short-range forces with varying tip radius, from 7 to 11 nm in 0.5 nm steps. The standard deviation was calculated for all fitting parameters (Table S2 values under brackets). For most of them, the resulting error was smaller than 10%. However, the amplitude of the monotonic part of the short-range force error was up to 30% in most cases. A similar approach was taken for impact analysis of the zero point calculation of the force. Conceding an error of ±0.1 nm for the zero position has quantitative consequences of 10% variation for gibbsite and 50% variation for silica in the absolute value of the amplitude of the monotonic short-range force. It is noteworthy to mention here that the absolute magnitude (and/or the sign) of a monotonically decaying short-range force (<1.5 nm) will strongly depend on the choice of DLVO model and Poisson−Boltzmann equation boundary conditions.[11,38,44,68−70] For instance, the standard Poisson−Boltzmann theory that does not take into account effects like ion size, ionic chemical nature, polarizability, and solvation of ions at distances lower that ∼1.5 nm will strongly overestimate the ion concentration (reaching unphysical values) and monotonically decaying force.[68] On the other hand, the oscillatory hydration force, which is the key aim of this work, is less affected (less that 15%) by the choices of the DLVO part and uncertainty of the tip radius or zero tip sample position.

https://doi.org/10.1021/acs.langmuir.1c02077
Langmuir 2022, 38, 914−926

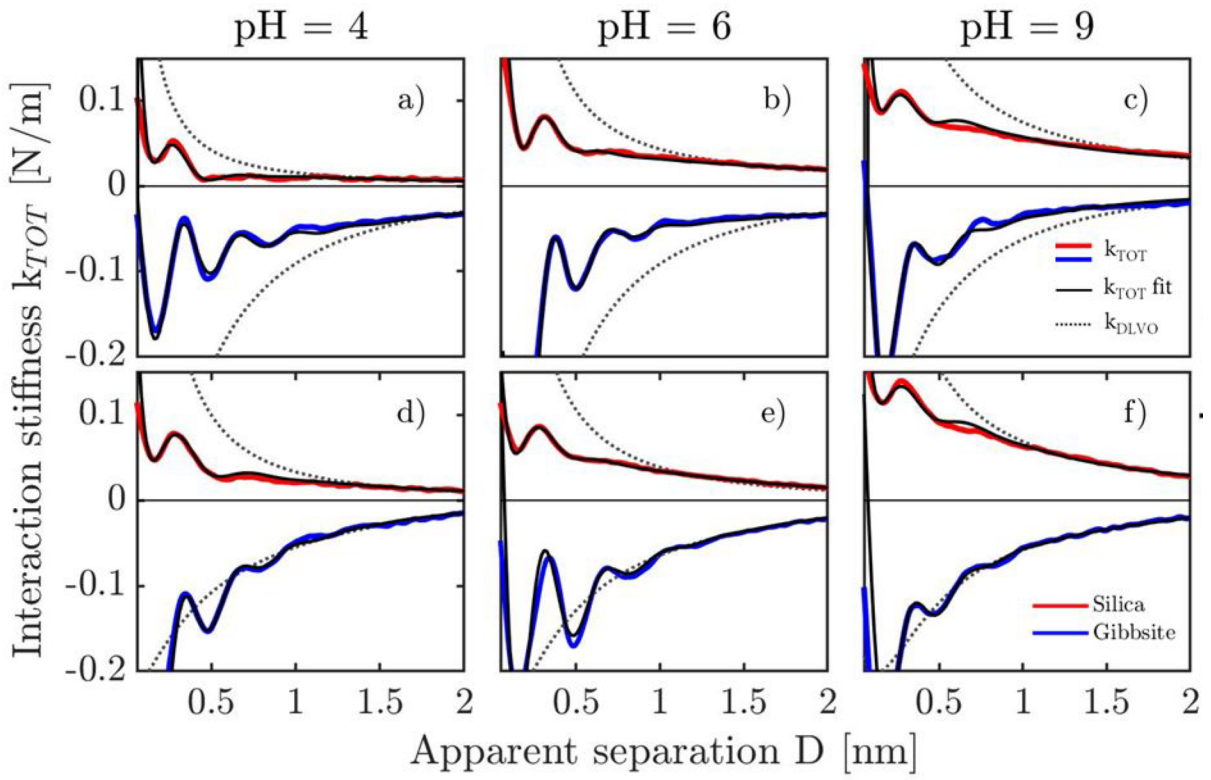

Figure 2. Average interaction stiffness from the 10 individual approaches for 10 (top) and 100 mM (bottom) NaCl at various pH values. Black solid lines are the best fits using a function consisting of a superposition of a DLVO interaction fit (k_{DLVO}), monotonic short-range force (k_{SR_MON}), and oscillatory hydration force (k_{HYD_OSC}) (eq 6 in Methods and Materials). Dotted black lines are the DLVO interactions.

3. RESULTS AND DISCUSSION

3.1. Macroscopic Characterization of a Nanoparticle. The results presented below (hydration and DLVO forces) on the same gibbsite particle were measured using noncontact amplitude-modulation atomic force microscopy (AM-AFM). All 3D force distance maps were measured on the same gibbsite particle on a silica substrate in various electrolyte solutions using the same silica tip with a radius of 9 ± 2 nm.

The gibbsite [$Al(OH)_3$] nanoparticles have a typical plate-like pseudohexagonal morphology with lateral dimensions ranging from 100 to 500 nm and heights from 5 to 20 nm (cross section in Figures 1a, 1b, and S1). The majority of the (001) basal plane of the nanoparticles displays 20−100 nm wide smooth terraces (Figures 1a and S1) separated by irregular areas containing steps and other defects[43,45,71] (Figures 1a and S1). Close to the edge of the particles, the density of the surface imperfections increases.[71]

3.2. Three-Dimensional Force Field Measurements. In the line representation of the force−distance curves (Figure 1c and 1d), three regions can be distinguished: (1) 7 > D > 1.5 nm, (2) 1.5 > D > 0.1 nm, and (3) D < 0.1 nm. In region 1, a monotonic attraction on gibbsite and repulsion on silica are observed. This force is caused by the electrostatic double layer (EDL). It decays exponentially with a decay of 2.6 nm (Figure S2), which agrees with the expected Debye screening length (3 nm at 10 mM NaCl).

Figure 1a shows a 2D projection of the force gradient (extracted from the 3D map at 2 nm separation) at pH 6 and 10 mM NaCl. The EDL interactions are homogeneous on silica (red) and rather heterogeneous on gibbsite (blue and green), consistent with our previous observations.[43−45] The forces are less attractive near topographic defects and near the rim of the particle.[43−45] The silica tip is negatively charged at pH > 3, which implies that the gibbsite surface is positively charged and the silica substrate is negatively charged. These results agree with earlier works, where larger tips (>25 nm) were used.[43−45] Therefore, we do not discuss the EDL forces and diffuse layer charge of gibbsite and silica extensively here.[43−45]

Measurements using a 9 nm tip allow us to uncover new insights in regions 2 and 3, which is the range of non-DLVO interactions. From the line representation of the force−distance (FD) curves (Figure 1c and 1d) at separations of 1.5 nm > D > 0.1 nm, an oscillatory (non-DLVO) force with up to three maxima ∼0.35 nm apart is clearly visible. The oscillatory force profile is indicative of ordered water layers and was not detected in earlier reports where larger tips were used.[43−45] In region 3, a strong repulsive force in the constant compliance region is detected. Commonly the oscillatory force or structural hydration force is measured on atomically smooth surfaces like mica and calcite.[17,48,72] Here, we were able to detect the oscillatory hydration force on the gibbsite crystalline basal plane and as well on amorphous silica substrate.

On gibbsite, more than one-half (∼60%) of the FD curves show oscillations and are primarily located on topographically smooth terraces as indicated by the circles in Figure 1a. On silica, only ∼10% of the FD curves show oscillations, which are randomly distributed across the sample (crosses on Figure 1a). In the rest of the sample locations, the FD curves display a monotonically decaying non-DLVO force in region 2 (Figure 1d). Here, the water molecules are not sufficiently ordered into discrete layers to present multiple energy barriers to the approaching nanoscale tip.

https://doi.org/10.1021/acs.langmuir.1c02077
Langmuir 2022, 38, 914−926

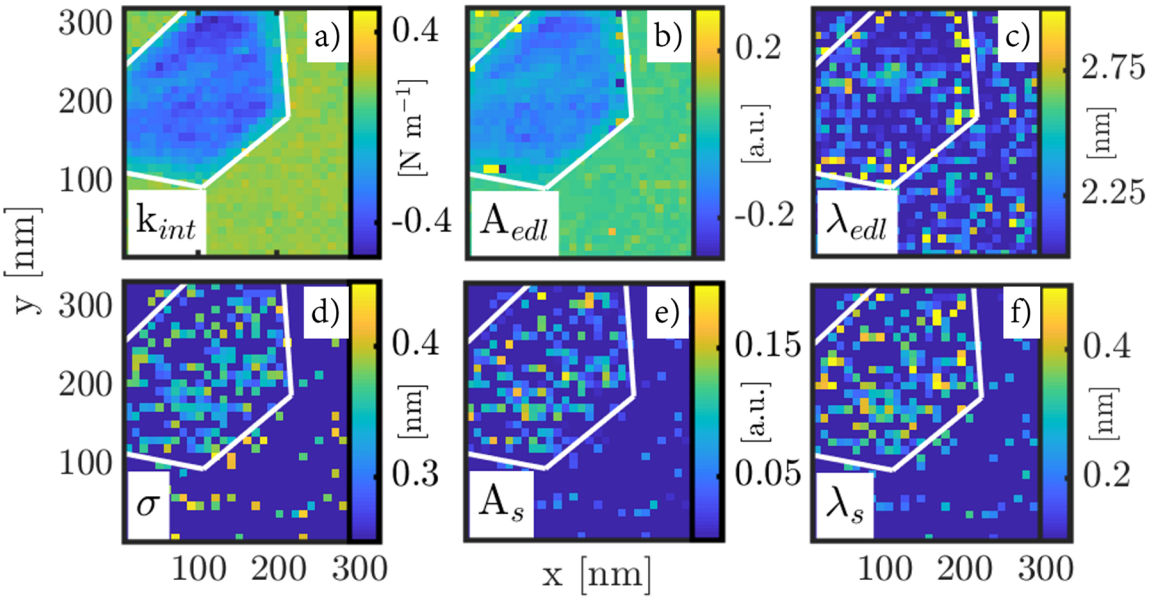

Figure 3. Fitting parameters for gibbsite on silica in a 10 mM NaCl pH 6 solution using eq 6. Top row shows the total interaction stiffness (k_{int}) at 2 nm from the surface (a) and amplitude (A_{EDL}) and decay length (λ_{EDL}) of the electric double-layer force (b and c). Bottom row shows the height and oscillation period (σ) (d), amplitude (A_{osc}) force (e), and decay lengths (λ_{osc}) (f) of the oscillatory hydration force.

It is important to emphasize that the AFM tip size, shape, and geometry of the tip apex (and as well hydration) may affect the oscillations in the hydration forces.[17,51,73] Generally, increasing the tip size and/or roughness (random and periodic) leads to an "averaging" of the oscillatory forces over the tip area, giving smaller magnitude oscillations in the force curve. The use of a sharper tip could lead to a higher amplitude and number of FD curves with an oscillatory profile (less smoothening of oscillations by the tip size effect), but this will compromise for the EDL force sensitivity. Yet, a relative comparison of materials hydration (silica vs gibbsite) and the influence of fluid composition on the structural hydration forces will stand independent of the tip.

3.3. Surface Force: Effect of pH and Ions Concentration. The same distinct characteristics of a long-range EDL and pronounced oscillatory interaction stiffness at a separation below 1.5 nm are observed in measurements at pH 4, 6, and 9 with 10 and 100 mM NaCl solutions (Figure 2). Solid colored lines in Figure 2 represent the average force gradient of 10 individual FD approaches that display an oscillatory behavior extracted from 3D force. The individual FD approaches are exclusively selected from topographically smooth terraces of gibbsite particle basal planes. All 3D force maps are recorded on the same gibbsite particle with the same probe, and great care was taken to guarantee that the tip size does not change during the measurements (see Methods and Materials for details). The force gradients at the beginning and after completing all 3D force maps overlap, indicating that the tip size did not change during the experiment (Figure S3). Particle surface features do not display visible roughening/degradation during the experiment (Figure S4). Therefore, all changes in the force strength and decay length (DLVO and hydration) at different fluid compositions are not a result of the tip or sample (silica and gibbsite particle) degradation effect.

Data presented in Figures 1 and 2 clearly indicate that a SiO_2 tip with a radius of 9 ± 2 nm is suitable for simultaneously mapping the oscillatory hydration and DLVO forces at the level of a single nanoparticle under various fluid conditions.

3.4. Fitting of Force−Distance Curves. Analysis of the 3D force maps using Derjaguin−Landau−Verwey−Overbeek theory with charge regulation (DLVO-CR) (see Methods and Materials section) allows one to quantify the 2D spatial distribution of the diffuse layer surface charge of the silica−gibbsite sample (Figure 4). The measurements at concentrations of 10 and 100 mM NaCl and pH values of 4, 6, and 9 reveal a decrease of the positive surface charge of the gibbsite basal plane and an increase of the negative surface charge of silica with increasing pH, which is good in agreement with expectations and earlier reports[43−45] (Figure 4). The DLVO theory with charge regulation can accurately describe the experimental force−distance curves only down to a separation distance of about 1.5−2 nm[43−45] (for both silica and gibbsite black dotted lines in Figure 2). Therefore, below 1.5 nm, oscillatory and monotonically decaying non-DLVO forces are present. The additional non-DLVO interaction (D < 1.5 nm) can be modeled with an empirical function consisting of the combination of a monotonically decaying exponential function ($k_{SR\_MON}(D)$) and a decaying oscillatory contribution ($k_{HYD\_OSC}(D)$) (see eq 6 in Methods and Materials). The improved model allows us to fit the total interaction stiffness (k_{TOT}) down to separations of ∼0.15 nm (solid black lines in Figure 2). The oscillatory force with a periodicity close to the size of a water molecule described by an exponentially decaying cos function is typically ascribed to the force required to displace layers of structured water molecules and therefore is called a oscillatory hydration force. The monotonically decaying short-range force (k_{SR_MON}) strength depends on the choice DLVO model. As extensively explained in the work of Ben-Yaakov and Podgornik,[68] at a separation below 1.5−2 nm, it is difficult or perhaps impossible to decouple the total monotonically decaying force into various well-defined separate contributions like DLVO and/or non-DLVO forces[70,71] because one cannot develop a universal Poisson−

https://doi.org/10.1021/acs.langmuir.1c02077
Langmuir 2022, 38, 914−926

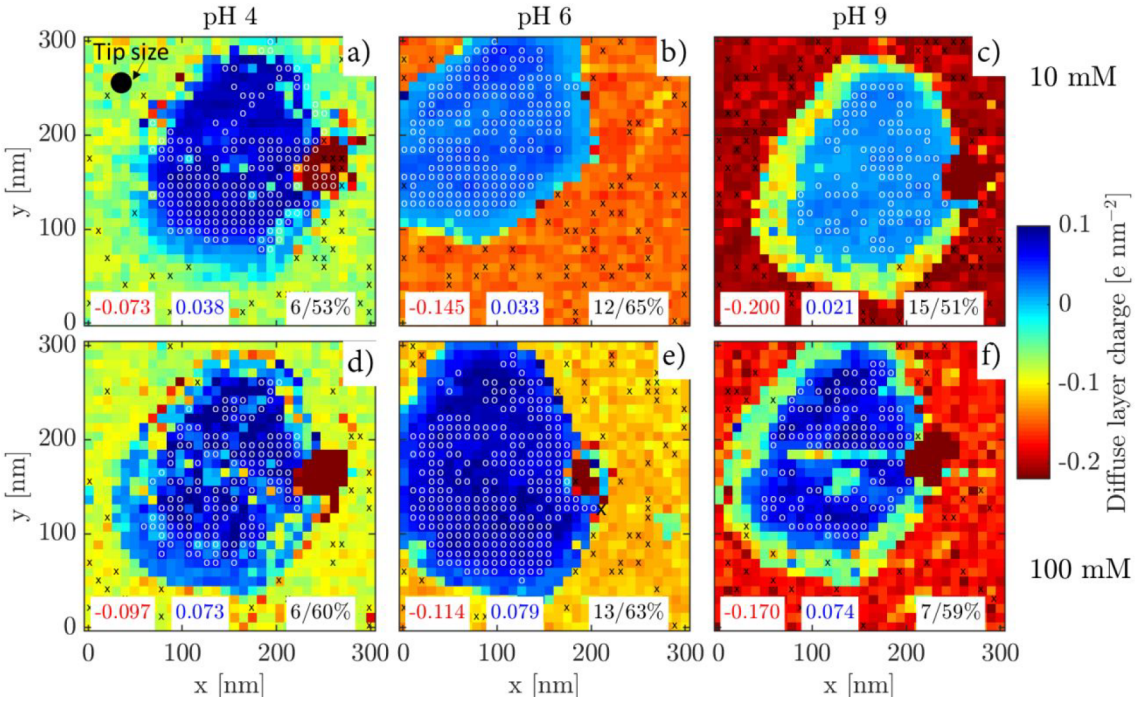

Figure 4. Diffuse layer charge maps of the same gibbsite particle on silica in various electrolyte solutions. Bottom left corner indicates the average diffuse layer charge for silica (red) and gibbsite (blue) extracted from smooth terraces. Bottom right shows the percentage of approaches that show oscillatory behavior on silica (left) and gibbsite (right). White circles and black crosses indicate the locations of FD approaches with oscillatory behavior on gibbsite and silica, respectively.

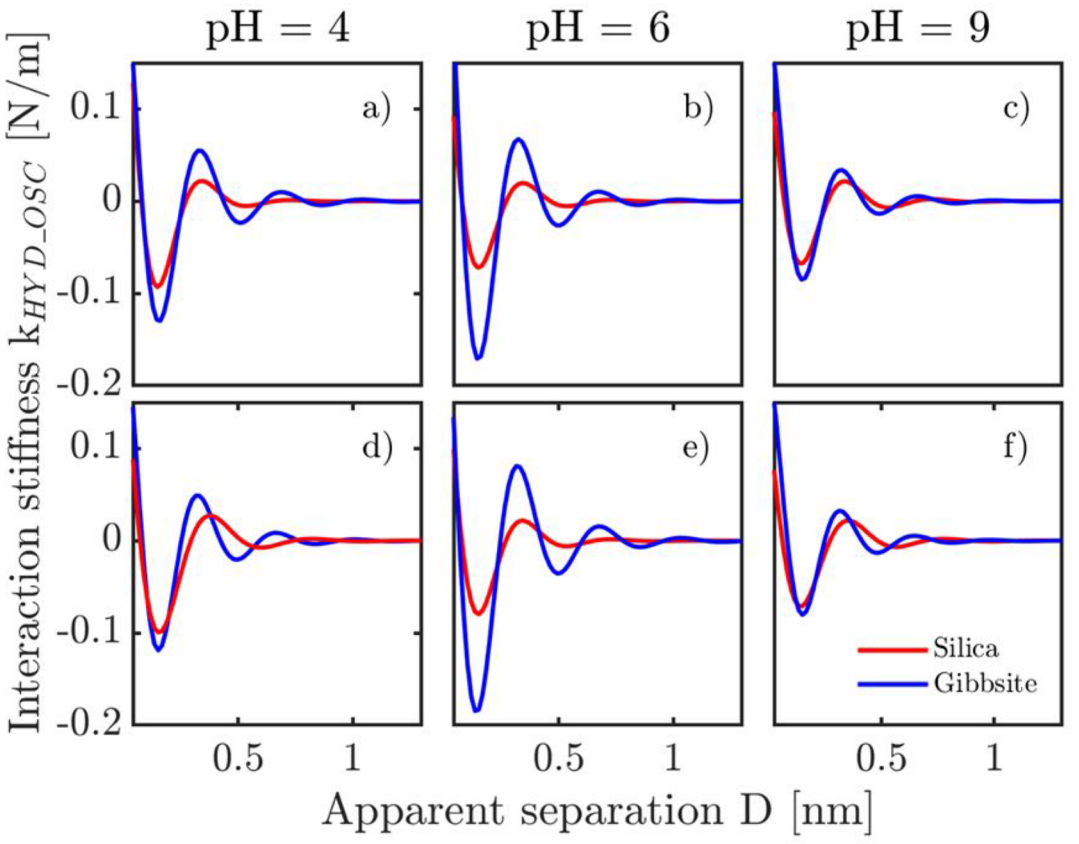

Figure 5. Structural hydration force gradient as a function of fluid composition. Top row is 10 mM NaCl, and bottom row is 100 mM NaCl. Decay length of the oscillatory hydration force for silica is λ_{osc} = 0.12 ± 0.01 nm. For gibbsite, λ_{osc} = 0.23 ± 0.02 nm. Periodicity of oscillatory hydration forces for gibbsite is σ = 0.34 ± 0.01 nm. For silica, σ = 0.4 ± 0.02 nm (see also Table S2).

https://doi.org/10.1021/acs.langmuir.1c02077
Langmuir 2022, 38, 914−926

Boltzmann theory accounting for all nonelectrostatic effects (ionic chemical nature, size, charge, polarizability, and solvation). Hence, here, k_{SR_MON} is considered as simply an empirical correction factor to the DLVO force at a separation of $D < 1.5$ nm.[1,38,42,6] The oscillatory hydration force is very robust and unaffected by the choice of the DLVO model, and therefore, the following discussion is focused only on the oscillatory hydration force, the EDL force, and their correlation with the surface charge.

The parameters (strength, decay length of the EDL and oscillatory hydration forces, oscillatory wavelength) extracted from data fitting at different fluid compositions are listed in Table S2. Spatial 2D distributions of the fitting parameters across silica−gibbsite sample are plotted in Figure 3. Individual components (k_{HYD_OSC}, k_{EDL}) of the total force gradient (k_{TOT}) are shown in Figures 3, 5, and S5. Analysis of the AFM data shows that the EDL force gradient between the SiO_2 tip and the SiO_2 substrate is repulsive and increases in strength (Table S2) with increasing pH and NaCl concentration (Figure S5). This is a result of an increasingly negative charge of the silica (Figure 4) as the fraction of deprotonated SiO^- groups rises with increasing pH and NaCl concentration.[43−45] On gibbsite, the EDL force is attractive (positive diffuse layer charge) under all investigated conditions and decreases with increasing pH from 4 to 9 (A_{EDL} in Table S2 and Figure S5).[43−45] The decay length of the EDL interaction decreases from 2.4 ± 0.4 to 1.07 ± 0.17 nm with increasing salt concentration from 10 to 100 mM (similar to the Debye length, λ_D = 3 and 0.96 nm). As expected, the experimental decay length is independent of the surface properties and the sign of the surface charge (see Figure 3 and Table S2). The small deviations from the theoretically calculated Debye lengths at low concentrations are most probably due to the lower force sensitivity at large separations with rather the sharp tip.

The decay length of the oscillatory hydration force for silica is λ_{osc} = 0.12 ± 0.01 nm (Table S2). For gibbsite, the value is larger, 0.23 ± 0.02 nm, indicating a thicker interfacial hydration layer. Even though the error bars are rather large, especially for silica, the present data (Table S2) suggest that the decay length of the oscillatory hydration forces does not vary significantly with salt concentration and pH but does depend on the substrate material. This suggests that the behavior of the hydration force is not caused by continuum electrostatics, as in classical colloid science (DLVO theory), but by more local forces involving the chemical details of the surface. This agrees with the recent report of van Lin et al.,[47] where the decay length of the oscillatory hydration force (oscillatory ≈ 0.2 ± 0.08) between a sharp silica tip and a mica surface was also found to be independent of fluid composition (pH and monovalent salts concentration from 0.001 to 4 M).

On gibbsite, three hydration layers can be distinguished, whereas on silica only two are visible with a smaller amplitude (A_{HYD_OSC} in Table S2, Figure 5). The gibbsite interfacial hydration is consistent with the experimental[74−76] observation and simulations[77,78] on isostructural surfaces such as the gibbsite facet of kaolinite and the (0001) faces of α-Al_2O_3 or α-Fe_2O_3. The AFM spectroscopy results along with the MD simulation reported by Arguris[74] and Ashby[76] and the X-ray reflectivity experiments of Catalano[75] at the (0001) hydroxylated α-Al_2O_3 substrate also report oscillatory hydration forces and three hydration layers extending up to ∼10 Å from the substrate, as observed here (Figure 5). Our data also agree with the DFT and MD simulations of Hu and Michaelides[77] and Chen and Liu,[78] indicating that the hydrated film on the kaolinite gibbsite facet surface is composed of about 3 hydrogen-bonded layers of water molecules with a thickness of ∼8−10 Å.

The average distance (σ in Table S2) between the adjacent hydration layers calculated using a periodic cosine function for gibbsite is 0.34 ± 0.01 nm. The values are rather independent of solution pH and NaCl concentration. For silica, these distances are substantially larger, namely, 0.4 ± 0.02 nm (Table S2). Note that the experimental data (deviation in the separation distance between the black and the red/blue lines in Figure 2) reveal that the separation between the hydration layers does not strictly maintain a constant periodicity but increases at larger distances from the surface. This is consistent with the X-ray reflectivity measurements and simulated interfacial water structures.[20] The increased layer spacing is indicative of reduced ordering within the hydration layers, and it is constant for hard-sphere liquids.[22,41] The amplitude and periodicity of the oscillatory hydration forces are typically associated with organization of water within the hydration layers. A higher oscillation amplitude and a closer periodicity to the diameter of the water molecule means a higher strength/order of the hydrogen-bond (HB) network between water molecules within ordered hydration layers.[20] Thus, the thickness and organization of water within the gibbsite hydration layers is higher compared to that of the amorphous silica surface.

There are at least two possible reasons for this: first, the amorphous silica surface is not as smooth as the crystalline surface of gibbsite.[20] Therefore, the ∼2 Å of surface roughness may overwhelm the layering of the water molecules and the oscillatory hydration force. Second, the different distribution and distance between the water hydrogen-bonding sites (OH groups) could be responsible for the dissimilar hydration structures observed on the two surfaces.[20] Amorphous silica has ∼5 OH groups/nm^2. The density of the proton reactive sites (OH) (i.e., can form a hydrogen bond with water molecules) on the basal plane of gibbsite is ∼13/nm^2, which is twice that for amorphous silica.[20,79,80] Therefore, for silica, these sites are relatively far from each other (∼0.5 nm) as compared to those for gibbsite (∼0.3 nm).[20,74] According to Phan and Striolo,[21,80] a higher density and proximity of OH groups, where water molecules can preferentially adsorb and reside, would give rise to (i) a higher density of water molecules in the hydration layers in the directions perpendicular and parallel to the surfaces, (ii) a higher density and strength of hydrogen bonds between the water molecules within the hydration layers in addition to the bonds with the substrate, and (iii) a larger residence time of water molecules near the surfaces. Altogether, this would lead to more organized hydration layers on gibbsite as compared to silica and, therefore, to a higher amplitude of oscillatory hydration forces, as observed in our measurements (Figure 5).

The gibbsite diffuse layer charge of the smooth terraces decreases from +0.038 to +0.021 e/nm^2 with a pH increase from 4 to 9 at 10 mM NaCl (Figure 5). On the other hand, the order within the hydration layers on gibbsite, as expressed by the strength A_{HYD_OSC}, seems to be most pronounced at pH 6 (Figure 5). In contrast, on silica, the strength of the oscillatory hydration force is found to be rather independent of fluid composition, while the diffuse layer charge increases by more than a factor of 2 (from −0.073 to −0.2 e/nm^2) when the pH changes from 4 to 9. As indicated with the circles and crosses

https://doi.org/10.1021/acs.langmuir.1c02077
Langmuir 2022, 38, 914−926

in Figure 4, the surface charge variation does not affect the number and spatial distribution of forces that exhibit an oscillatory profile. On gibbsite, more than one-half (~60%) of the force curves display oscillatory character, preferentially at regions with flat topography (Figure 4). This number is rather independent of electrolyte composition. In areas with topographic defects, force oscillations are smeared out, leaving only a monotonic component of non-DVLO force. On silica, despite the homogeneous surface charge distribution and surface roughness, the structural hydration forces are present on ~10% random locations only (Figure 4).

Thanks to the simultaneous detection of EDL and hydration forces, we reveal that the diffuse layer charge and oscillatory hydration force are not correlated and respond very differently to variations in pH and salt concentration (Figures 4 and 5). This can be rationalized in the following way. Also, the origin of the charge on the gibbsite basal plane is a matter of debate;[43,45,61,63,81−83] the absolute degree of ionization of the smooth terraces of the basal plane of gibbsite, as probed on the colloidal scale, is rather small, on average +0.05 e/nm^2 under the conditions studied here (Figure 4). This corresponds to only ~1 positive charge in ~40 unit cells.[40,43,45] In other words, the average distance between charged sites on the gibbsite surface is of the order of a few nanometers and, thus, substantially larger than the water−water correlation length of λ = 3−5 Å, i.e., the distance over which structuring of water propagates within the solution. This separation of length scales suggests that the gibbsite colloidal scale surface charge cannot be the dominant factor for the short-range organization of water molecules near surfaces and, thus, for structural hydration forces. It is more plausible that the hydration structure originates from molecular scale hydrogen bonding of water molecules with −OH groups above the aluminum (Al) atom. Recent computational studies (molecular dynamics and density functional theory)[84−87] have shown that a gibbsite basal plane has three −OH groups (proton donors) pointing into the solution. These groups strongly prefer the interaction with H_2O molecules. The other three −OH groups are almost parallel to the surface, being not easily accessible for H_2O and are overall proton acceptors. This leads to a highly organized first water layer with overall O of the water molecules pointing toward the surface following the gibbsite hexagonal lattice arrangements. This strong order induces additional ordering in subsequent water layers up to 1 nm above the surface, as suggested by the range of the measured force oscillations (Figure 5). Apparently, the change in the pH of the solution from 6 to 4 or 9 changes the interaction of water molecules with the OH groups of the gibbsite surface and/or H bonding to the neighbors and destabilizes the ordering within the interfacial hydration layers, reducing the amplitude of the measured oscillatory hydration forces (Figure 5). One possible explanation is the multisite complexation (MUSIC) model developed by Bickmore et al.[82] According to the MUSIC model, one of six different types of doubly coordinated hydroxyl groups ($\equiv Al_2OH$) in each unit cell should have a pK value of 5.2 and could deprotonate/protonate at pH higher/lower than 6. Therefore, at pH 9 these sites transform from proton donors to only proton acceptors. As a consequence, the water molecules are forced to reorient with respect to their neighbors and thereby destabilize the hydrogen bonding of the interfacial water layers. This could explain the reduced strength of the oscillatory forces at high pH. At pH 4, the protonation of these sites changes their interaction with water as well, weakening the hydrogen bonding of the hydration layers. However, the presence of microscopic defects and their associated singly coordinated −OH groups (designated $\equiv$AlOH), with a p$K \approx 6$ within the probing area, or more complex processes such as specific ion adsorption or reorientation of surface OH groups can lead to the same effect.[40,71]

For silica, the origin of the hydration forces is a controversial topic, despite extensive studies for over a century.[14,42,88−93] Except the work of Fielden et al.,[93] in all previous studies, only monotonic non-DLVO forces have been measured experimentally. Therefore, often this non-DLVO force was assigned to elastic deformation of polysilicic acid chains (or "silica hairs") protruding from the silica surface[88,89,92,94] rather than to the hydration structure.[89−91] In work by Fielden et al.,[93] the oscillatory forces with a periodicity of ~0.9 nm were measured only at concentrations above 1 M $CaCl_2$ and were assigned to squeezing out of alternating layers of cations and anions, not to water. In 1 M NaCl solution, only a monotonic non-DLVO repulsive force was detected, as observed by Chapel,[91] Grabbe and Horn et al.,[90] Ducker et al.,[95,96] and Vigil et al.[92] In our measurements, the oscillatory character with the periodicity close to a water molecule clearly demonstrates that the force originates from structured hydration layers.

There is currently some disagreement on whether the short-range monotonic hydration force is dependent on the silica surface charge. Ducker et al.'s[95,96] results indicate that the force increases with surface charge. On the other hand, Horn et al.[89,90] and Chapel[91] indicate a constant additional monotonic non-DLVO force independent of solution conditions (pH and ionic strength), as observed here. The independence of the hydration force of pH and NaCl concentration suggests that charged SiO^- groups do not significantly contribute to the silica structural hydration effects (Figure 5). Otherwise, the increase of pH of the bulk water and thus the degree of silica surface charge would lead to an increased strength of the hydration force,[95] which we do not observe in our measurements. Therefore, consistent with earlier studies of Horn et al.[89,90] and Chapel,[91] recent MD simulations, and a few experiments, we attribute the origin of the hydration structure and force primarily to hydrogen bonding of water molecules to undissociated silanol (Si−OH) groups on the surface.[30,31,79,97−99]

This interpretation is consistent with the fact that the large majority (>75%) of surface silanol (Si−OH) groups does not dissociate even at a pH as high as 10. For the fluid compositions investigated here, the fraction of deprotonated silanol groups increases only from 0.2% to 2% per nm^2 between pH 4 and 9 for 100 mM NaCl, thus leaving the vast majority of silanol groups protonated or complexed with a cation (at pH 9 and 100 mM NaCl the fraction of surface SiO^-Na^+ complexes is <30%).[44] Computational studies by Cimas et al.[100] and Cyran et al.[31] showed that the amorphous silica surface in contact with water typically exposes siloxane (Si−O−Si), silanol (Si−OH), and above the isoelectric point (pH ≈ 3) a few silanolate ($Si-O^-$) groups. Further, silanol groups, depending of their orientation (15% in plane and 85% out of plane"), can donate a H bond to a water molecule, accept a H bond, or be simultaneously acceptor/donor.[15,31] This leads to a highly organized first water layer with a net dipole moment where the positive end of the water molecule points toward the surface. Subsequently, this first ordered water layer induces additional ordering in subsequent water

https://doi.org/10.1021/acs.langmuir.1c02077
Langmuir 2022, 38, 914−926

layers up to 1 nm above the surface, as suggested by the range of the measured force oscillations (Figure 5). The organization and range of subsequent hydration layers is controlled by water−water hydrogen bonding.

The oscillatory hydration forces in the present system do not display any appreciable dependence on NaCl concentration (Figures 5). This can be explained by the presence of very few silanol groups that are complexed with Na^+. It is less than 30% $Si-O^-Na^+$ even at pH 9 and 100 mM NaCl.[44] Hence, the silica (and gibbsite) surfaces are primarily covered by water molecules interacting with surface−OH groups and not by counterions, and therefore, direct surface hydration is more important for hydration forces than counterion density and hydration. In addition, recent simulations show that, specifically, $Si-O^-Na^+$ complexes only slightly reduce the silanolate−water coordination number from 2.83 (pure water) to 2.67 in 200 mM NaCl.[98,99] Note that the hydration structure and hydration forces (monotonic and oscillatory) may be very system specific and may depend on the surface structure, surface charge density, site density where ions/water molecules adsorb, ion surface coverage, bulk/interfacial ion hydration, and direct ion−substrate interaction, etc. For example, the mica surface, independent of pH and at low salt concentration, is almost fully covered with cations that compensate for the strong intrinsic negative surface charge (0.5 e/nm^2) caused by isomorphic substitution of Si by Al atoms.[20,52] Moreover, mica does not have undissociated hydroxyl groups, and therefore, water molecules and cations compete for the same surface sites (ditrigonal cavities).[19,101]

As a final remark, the locations (∼10% random) where forces display an oscillatory profile on silica (Figure 5) could be most likely due to less "microscopic" surface roughness that is not detectable with the 9 nm tip used. Alternately, intermingled regions (∼2 nm) of ordered and disordered interfacial water could be due to a patchy and nonuniform distribution of silanol (Si−OH)-rich (hydrophilic sites, high ability to both accept and donate H bonds) and siloxane (Si−O−Si)-rich (hydrophobic sites, weakly accept H bonds) domains, as reveled by MD simulations.[31,97,102,103] As pointed out in earlier work by Sivan et al.[104] and recent work by Bourget et al.,[97] the relative strength of silanol (Si−OH)−water bonding (vs water−water bonding) and the spatial distribution with respect to the siloxane (Si−O−Si) groups can modulate not only the hydration and microscopic hydrophobicity of the silica surface but also the ion adsorption behavior and other interfacial processes. However, more detailed experiments (different tip size and hydroxylation state of silica) are required to know whether the regions with forces that display oscillations are (Si−OH) rich or an effect of the intrinsic disorder of the amorphous silica surface.

4. CONCLUSIONS

AFM with intermediate-sized tips allows one to simultaneously quantify oscillatory hydration forces caused by the discreteness of water molecules and continuum of DLVO forces at a heterogeneous mineral−electrolyte interface consisting of a crystalline gibbsite nanoparticle adsorbed on an amorphous silica substrate. Measurements at NaCl concentrations of 10 and 100 mM and pH values of 4, 6, and 9 reveal a decrease of the positive surface charge of the gibbsite basal plane and an increasingly negative surface charge of silica with increasing pH in agreement with expectations. In contrast, the strength of the simultaneously measured oscillatory hydration forces varies only weakly with pH, suggesting that the microscopic origin of these forces is hardly affected by the surface charge density or surface potential (and charge density) that controls both the continuum of DLVO forces at tip−sample separations of 1 nm and beyond as well as electrokinetic measurements. Our measurements also show that the strength of the oscillatory hydration forces is more pronounced on crystalline gibbsite basal planes as compared to the amorphous silica surface, suggesting that oscillatory hydration forces involve more than a simple geometric packing of water molecules. While a contribution due to the slight differences in surface roughness cannot be excluded, we argue that differences in the ability of the perfectly periodic gibbsite lattice with its 2−3 times higher density OH groups per surface area lead to a stronger degree of organization of the hydration layers and thereby to stronger oscillatory forces. These effects seem to be independent from the strong polarization effects of interfacial water reported in recent SFG measurements that do scale with the surface potential. We anticipate that the physical insights presented in this work will help to disentangle the relative importance of short-range hydration and DLVO forces for a variety of materials and phenomena involving both colloidal and molecular scale processes.

■ ASSOCIATED CONTENT

Supporting Information

The Supporting Information is available free of charge at https://pubs.acs.org/doi/10.1021/acs.langmuir.1c02077.

Surface complexation equations used in force analysis based on the charge regulation-complemented DLVO theory; parameters (strength, decay length of the EDL and oscillatory hydration forces, oscillatory wavelength) extracted from fitting the interaction forces at different fluid compositions; AFM images and interaction forces on the silica−gibbsite system before and after completion of the experiment; electric double-layer force as a function of fluid composition (PDF)

■ AUTHOR INFORMATION

Corresponding Author

Igor Siretanu − *Physics of Complex Fluids Group and MESA+ Institute, Faculty of Science and Technology, University of Twente, 7500 AE Enschede, The Netherlands;* orcid.org/0000-0002-5741-9561; Phone: ++31 (0)53 489 3089; Email: i.siretanu@utwente.nl; Fax: ++31 (0)53 489 1096

Authors

Aram Klaassen − *Physics of Complex Fluids Group and MESA+ Institute, Faculty of Science and Technology, University of Twente, 7500 AE Enschede, The Netherlands*

Fei Liu − *Physics of Complex Fluids Group and MESA+ Institute, Faculty of Science and Technology, University of Twente, 7500 AE Enschede, The Netherlands*

Frieder Mugele − *Physics of Complex Fluids Group and MESA+ Institute, Faculty of Science and Technology, University of Twente, 7500 AE Enschede, The Netherlands;* orcid.org/0000-0003-3824-3617

Complete contact information is available at: https://pubs.acs.org/10.1021/acs.langmuir.1c02077

Notes

The authors declare no competing financial interest.

■ ACKNOWLEDGMENTS

The authors thank Albert Philipse for providing a gibbsite sample. This work is part of the research program Rock-on-a-Chip (project no. i40), which is cofinanced by The Netherlands Organization for Scientific Research (NWO) and by the Exploratory Research (ExploRe) programme of BP plc. BP Exploration Operating Co. Ltd. is thanked for permission to publish this paper.

■ REFERENCES

(1) Israelachvili, J. N. *Intermolecular and surface forces*, 3rd ed.; Elsevier Amsterdam, 2011; pp 191−499.
(2) Honig, B.; Nicholls, A. Classical electrostatics in biology and chemistry. *Science* **1995**, *268* (5214), 1144−1149.
(3) Ledezma-Yanez, I.; Wallace, W. D. Z.; Sebastián-Pascual, P.; Climent, V.; Feliu, J. M.; Koper, M. T. Interfacial water reorganization as a pH-dependent descriptor of the hydrogen evolution rate on platinum electrodes. *Nat. Energy* **2017**, *2* (4), 17031.
(4) Smit, B.; Reimer, J. A.; Oldenburg, C. M.; Bourg, I. C. *Introduction to carbon capture and sequestration*; World Scientific, 2014; Vol. *1*.
(5) Manciu, M.; Ruckenstein, E. Role of the hydration force in the stability of colloids at high ionic strengths. *Langmuir* **2001**, *17* (22), 7061−7070.
(6) Wennerstrom, H.; Vallina Estrada, E.; Danielsson, J.; Oliveberg, M. Colloidal stability of the living cell. *Proc. Natl. Acad. Sci. USA* **2020**, *117* (19), 10113−10121.
(7) Su, S.; Siretanu, I.; van den Ende, D.; Mei, B.; Mul, G.; Mugele, F. Facet-dependent Surface Charge and Hydration of Semiconducting Nanoparticles at Variable pH. *Adv. Mater.* **2021**, *33*, 2106229.
(8) Parsons, D. F.; Boström, M.; Nostro, P. L.; Ninham, B. W. Hofmeister effects: interplay of hydration, nonelectrostatic potentials, and ion size. *Phys. Chem. Chem. Phys.* **2011**, *13* (27), 12352−12367.
(9) Klein, J. Hydration lubrication. *Friction* **2013**, *1* (1), 1−23.
(10) Voïtchovsky, K.; Kuna, J. J.; Contera, S. A.; Tosatti, E.; Stellacci, F. Direct mapping of the solid-liquid adhesion energy with subnanometre resolution. *Nat. Nanotechnol.* **2010**, *5* (6), 401−405.
(11) Israelachvili, J. N. *Intermolecular and surface forces*; Academic Press, 2015.
(12) Langmuir, I. The role of attractive and repulsive forces in the formation of tactoids, thixotropic gels, protein crystals and coacervates. *J. Chem. Phys.* **1938**, *6* (12), 873−896.
(13) Parsegian, V.; Zemb, T. Hydration forces: Observations, explanations, expectations, questions. *Current opinion in colloid & interface science* **2011**, *16* (6), 618−624.
(14) Valle-Delgado, J.; Molina-Bolivar, J.; Galisteo-Gonzalez, F.; Galvez-Ruiz, M.; Feiler, A.; Rutland, M. W. Hydration forces between silica surfaces: Experimental data and predictions from different theories. *J. Chem. Phys.* **2005**, *123* (3), 034708.
(15) Björneholm, O.; Hansen, M. H.; Hodgson, A.; Liu, L.-M.; Limmer, D. T.; Michaelides, A.; Pedevilla, P.; Rossmeisl, J.; Shen, H.; Tocci, G.; et al. Water at interfaces. *Chem. Rev.* **2016**, *116* (13), 7698−7726.
(16) Kanduč, M.; Schlaich, A.; Schneck, E.; Netz, R. R. Water-mediated interactions between hydrophilic and hydrophobic surfaces. *Langmuir* **2016**, *32* (35), 8767−8782.
(17) Fukuma, T.; Garcia, R. Atomic-and Molecular-resolution mapping of solid-liquid interfaces by 3D atomic force microscopy. *ACS Nano* **2018**, *12* (12), 11785−11797.
(18) Backus, E.; Schaefer, J.; Bonn, M. The mineral/water interface probed with nonlinear optical spectroscopy. *Angew. Chem., Int. Ed.* **2021**, *133*, 10574.
(19) Bourg, I. C.; Lee, S. S.; Fenter, P.; Tournassat, C. Stern layer structure and energetics at mica-water interfaces. *J. Phys. Chem. C* **2017**, *121* (17), 9402−9412.
(20) Striolo, A. From interfacial water to macroscopic observables: A review. *Adsorption Science & Technology* **2011**, *29* (3), 211−258.
(21) Monroe, J.; Barry, M.; DeStefano, A.; Gokturk, P. A.; Jiao, S.; Robinson-Brown, D.; Webber, T.; Crumlin, E. J.; Han, S.; Shell, M. S. Water Structure and Properties at Hydrophilic and Hydrophobic Surfaces. *Annu. Rev. Chem. Biomol. Eng.* **2020**, *11*, 523.
(22) Ludwig, M.; von Klitzing, R. Recent progress in measurements of oscillatory forces and liquid properties under confinement. *Curr. Opin. Colloid Interface Sci.* **2020**, *47*, 137−152.
(23) Brugman, S. J.; Raiteri, P.; Accordini, P.; Megens, F.; Gale, J. D.; Vlieg, E. Calcite (104) surface-electrolyte structure: A 3D comparison of surface X-ray diffraction and simulations. *J. Phys. Chem. C* **2020**, *124* (34), 18564−18575.
(24) Fenter, P.; Sturchio, N. C. Mineral-water interfacial structures revealed by synchrotron X-ray scattering. *Prog. Surf. Sci.* **2004**, *77* (5−8), 171−258.
(25) Velasco-Velez, J.-J.; Wu, C. H.; Pascal, T. A.; Wan, L. F.; Guo, J.; Prendergast, D.; Salmeron, M. The structure of interfacial water on gold electrodes studied by x-ray absorption spectroscopy. *Science* **2014**, *346* (6211), 831−834.
(26) Fenter, P.; Lee, S. S. Hydration layer structure at solid-water interfaces. *MRS Bull.* **2014**, *39* (12), 1056.
(27) Bourg, I. C.; Sposito, G. Molecular dynamics simulations of the electrical double layer on smectite surfaces contacting concentrated mixed electrolyte (NaCl-CaCl2) solutions. *J. Colloid Interface Sci.* **2011**, *360* (2), 701−715.
(28) Döpke, M. F.; Lützenkirchen, J.; Moultos, O. A.; Siboulet, B.; Dufrêche, J.-F. o.; Padding, J. T.; Hartkamp, R. Preferential adsorption in mixed electrolytes confined by charged amorphous silica. *J. Phys. Chem. C* **2019**, *123* (27), 16711−16720.
(29) Jena, K. C.; Covert, P. A.; Hore, D. K. The effect of salt on the water structure at a charged solid surface: Differentiating second-and third-order nonlinear contributions. *J. Phys. Chem. Lett.* **2011**, *2* (9), 1056−1061.
(30) Marchioro, A.; Bischoff, M.; Lutgebaucks, C.; Biriukov, D.; Predota, M.; Roke, S. Surface Characterization of Colloidal Silica Nanoparticles by Second Harmonic Scattering: Quantifying the Surface Potential and Interfacial Water Order. *J. Phys. Chem. C* **2019**, *123* (33), 20393−20404.
(31) Cyran, J. D.; Donovan, M. A.; Vollmer, D.; Siro Brigiano, F.; Pezzotti, S.; Galimberti, D. R.; Gaigeot, M.-P.; Bonn, M.; Backus, E. H. G. Molecular hydrophobicity at a macroscopically hydrophilic surface. *Proc. Natl. Acad. Sci. USA* **2019**, *116* (5), 1520−1525.
(32) Israelachvili, J. N.; Pashley, R. M. Molecular layering of water at surfaces and origin of repulsive hydration forces. *Nature* **1983**, *306* (5940), 249−250.
(33) Ma, L.; Gaisinskaya-Kipnis, A.; Kampf, N.; Klein, J. Origins of hydration lubrication. *Nat. Commun.* **2015**, *6* (1), 6060.
(34) Zachariah, Z.; Espinosa-Marzal, R. M.; Heuberger, M. P. Ion specific hydration in nano-confined electrical double layers. *J. Colloid Interface Sci.* **2017**, *506*, 263−270.
(35) Baimpos, T.; Shrestha, B. R.; Raman, S.; Valtiner, M. Effect of interfacial ion structuring on range and magnitude of electric double layer, hydration, and adhesive interactions between mica surfaces in 0.05−3 M Li+ and Cs+ electrolyte solutions. *Langmuir* **2014**, *30* (15), 4322−4332.
(36) Pashley, R. DLVO and hydration forces between mica surfaces in Li+, Na+, K+, and Cs+ electrolyte solutions: A correlation of double-layer and hydration forces with surface cation exchange properties. *J. Colloid Interface Sci.* **1981**, *83* (2), 531−546.
(37) Butt, H.-J. Measuring electrostatic, van der Waals, and hydration forces in electrolyte solutions with an atomic force microscope. *Biophysical journal* **1991**, *60* (6), 1438−1444.
(38) Trefalt, G.; Palberg, T.; Borkovec, M. Forces between colloidal particles in aqueous solutions containing monovalent and multivalent ions. *Curr. Opin. Colloid Interface Sci.* **2017**, *27*, 9−17.
(39) Trefalt, G.; Behrens, S. H.; Borkovec, M. Charge regulation in the electrical double layer: ion adsorption and surface interactions. *Langmuir* **2016**, *32* (2), 380−400.

https://doi.org/10.1021/acs.langmuir.1c02077
Langmuir 2022, 38, 914−926

(40) Franks, G. V.; Gan, Y. Charging behavior at the alumina-water interface and implications for ceramic processing. *J. Am. Ceram. Soc.* **2007**, *90* (11), 3373−3388.
(41) Ludwig, M.; von Klitzing, R. progress in measurements of oscillatory forces and liquid properties under confinement. *Curr. Opin. Colloid Interface Sci.* **2020**, *47*, 137.
(42) Diao, Y.; Espinosa-Marzal, R. M. Molecular insight into the nanoconfined calcite-solution interface. *Proc. Natl. Acad. Sci. U. S. A.* **2016**, *113* (43), 12047−12052.
(43) Siretanu, I.; Ebeling, D.; Andersson, M. P.; Stipp, S. S.; Philipse, A.; Stuart, M. C.; Van Den Ende, D.; Mugele, F. Direct observation of ionic structure at solid-liquid interfaces: a deep look into the Stern Layer. *Sci. Rep.* **2015**, *4*, 4956.
(44) Zhao, C.; Ebeling, D.; Siretanu, I.; van den Ende, D.; Mugele, F. Extracting local surface charges and charge regulation behavior from atomic force microscopy measurements at heterogeneous solid-electrolyte interfaces. *Nanoscale* **2015**, *7* (39), 16298−16311.
(45) Klaassen, A.; Liu, F.; Van den Ende, D.; Mugele, F.; Siretanu, I. Impact of surface defects on the surface charge of gibbsite nanoparticles. *Nanoscale* **2017**, *9* (14), 4721−4729.
(46) Kumar, N.; Andersson, M.; Van den Ende, D.; Mugele, F.; Siretanu, I. Probing the surface charge on the basal planes of kaolinite particles with high-resolution atomic force microscopy. *Langmuir* **2017**, *33* (50), 14226−14237.
(47) Van Lin, S. R.; Grotz, K. K.; Siretanu, I.; Schwierz, N.; Mugele, F. Ion-specific and pH-dependent hydration of mica-electrolyte interfaces. *Langmuir* **2019**, *35* (17), 5737−5745.
(48) Söngen, H.; Reischl, B.; Miyata, K.; Bechstein, R.; Raiteri, P.; Rohl, A. L.; Gale, J. D.; Fukuma, T.; Kühnle, A. Resolving point defects in the hydration structure of calcite (10.4) with three-dimensional atomic force microscopy. *Physical review letters* **2018**, *120* (11), 116101.
(49) Kuchuk, K.; Sivan, U. Hydration structure of a single DNA molecule revealed by frequency-modulation atomic force microscopy. *Nano Lett.* **2018**, *18* (4), 2733−2737.
(50) Kilpatrick, J. I.; Loh, S.-H.; Jarvis, S. P. Directly probing the effects of ions on hydration forces at interfaces. *J. Am. Chem. Soc.* **2013**, *135* (7), 2628−2634.
(51) Fukuma, T.; Reischl, B.; Kobayashi, N.; Spijker, P.; Canova, F. F.; Miyazawa, K.; Foster, A. S. Mechanism of atomic force microscopy imaging of three-dimensional hydration structures at a solid-liquid interface. *Phys. Rev. B* **2015**, *92* (15), 155412.
(52) Ricci, M.; Spijker, P.; Voïtchovsky, K. Water-induced correlation between single ions imaged at the solid-liquid interface. *Nat. Commun.* **2014**, *5* (1), 4400.
(53) Wierenga, A. M.; Lenstra, T. A.; Philipse, A. P. Aqueous dispersions of colloidal gibbsite platelets: synthesis, characterisation and intrinsic viscosity measurements. *Colloids Surf., A* **1998**, *134* (3), 359−371.
(54) Icenhower, J. P.; Dove, P. M. The dissolution kinetics of amorphous silica into sodium chloride solutions: effects of temperature and ionic strength. *Geochim. Cosmochim. Acta* **2000**, *64* (24), 4193−4203.
(55) Dietzel, M.; Böhme, G. The dissolution rates of gibbsite in the presence of chloride, nitrate, silica, sulfate, and citrate in open and closed systems at 20 C. *Geochim. Cosmochim. Acta* **2005**, *69* (5), 1199−1211.
(56) García, R. *Amplitude modulation atomic force microscopy*; John Wiley & Sons, 2011.
(57) Liu, F.; Zhao, C.; Mugele, F.; van den Ende, D. Amplitude modulation atomic force microscopy, is acoustic driving in liquid quantitatively reliable? *Nanotechnology* **2015**, *26* (38), 385703.
(58) Ninham, B. W.; Parsegian, V. A. Electrostatic potential between surfaces bearing ionizable groups in ionic equilibrium with physiologic saline solution. *Journal of theoretical biology* **1971**, *31* (3), 405−428.
(59) Behrens, S. H.; Borkovec, M. Exact Poisson-Boltzmann solution for the interaction of dissimilar charge-regulating surfaces. *Phys. Rev. E Stat Phys. Plasmas Fluids Relat Interdiscip Topics* **1999**, *60* (6), 7040.
(60) Dishon, M.; Zohar, O.; Sivan, U. From Repulsion to Attraction and Back to Repulsion: The Effect of NaCl, KCl, and CsCl on the Force between Silica Surfaces in Aqueous Solution. *Langmuir* **2009**, *25* (5), 2831−2836.
(61) Gan, Y.; Franks, G. V. Charging behavior of the Gibbsite basal (001) surface in NaCl solution investigated by AFM colloidal probe technique. *Langmuir* **2006**, *22* (14), 6087−6092.
(62) Butt, H. J.; Cappella, B.; Kappl, M. Force measurements with the atomic force microscope: Technique, interpretation and applications. *Surf. Sci. Rep.* **2005**, *59* (1−6), 1−152.
(63) Hiemstra, T.; Van Riemsdijk, W.; Bolt, G. Multisite proton adsorption modeling at the solid/solution interface of (hydr) oxides: A new approach: I. Model description and evaluation of intrinsic reaction constants. *J. Colloid Interface Sci.* **1989**, *133* (1), 91−104.
(64) Rosenqvist, J.; Persson, P.; Sjöberg, S. Protonation and charging of nanosized gibbsite (α-Al (OH) 3) particles in aqueous suspension. *Langmuir* **2002**, *18* (12), 4598−4604.
(65) Todd, B. A.; Eppell, S. J. Probing the limits of the Derjaguin approximation with scanning force microscopy. *Langmuir* **2004**, *20* (12), 4892−4897.
(66) Ho, R.; Yuan, J.-Y.; Shao, Z. Hydration force in the atomic force microscope: a computational study. *Biophysical journal* **1998**, *75* (2), 1076−1083.
(67) Lim, L. T.; Wee, A. T.; O'Shea, S. J. Effect of tip size on force measurement in atomic force microscopy. *Langmuir* **2008**, *24* (6), 2271−2273.
(68) Ben-Yaakov, D.; Andelman, D.; Harries, D.; Podgornik, R. Beyond standard Poisson-Boltzmann theory: ion-specific interactions in aqueous solutions. *J. Phys.: Condens. Matter* **2009**, *21* (42), 424106.
(69) Netz, R. R. Static van der Waals interactions in electrolytes. *Eur. Phys. J. E* **2001**, *5* (2), 189−205.
(70) Kuhn, S.; Rahe, P. Discriminating short-range from van der Waals forces using total force data in noncontact atomic force microscopy. *Phys. Rev. B* **2014**, *89* (23), 235417.
(71) Siretanu, I.; van den Ende, H.; Mugele, F. Resolving clay mineral surfaces-from periodic atomic structure to surface defects. *NANOSCALE 8* **2016**, *8*, 8220−8227.
(72) Fukuma, T.; Ueda, Y.; Yoshioka, S.; Asakawa, H. Atomic-scale distribution of water molecules at the mica-water interface visualized by three-dimensional scanning force microscopy. *Phys. Rev. Lett.* **2010**, *104* (1), 016101.
(73) Argyris, D.; Ashby, P. D.; Striolo, A. Structure and orientation of interfacial water determine atomic force microscopy results: insights from molecular dynamics simulations. *ACS Nano* **2011**, *5* (3), 2215−2223.
(74) Argyris, D.; Ho, T.; Cole, D. R.; Striolo, A. Molecular dynamics studies of interfacial water at the alumina surface. *J. Phys. Chem. C* **2011**, *115* (5), 2038−2046.
(75) Catalano, J. G. Weak interfacial water ordering on isostructural hematite and corundum (0 0 1) surfaces. *Geochim. Cosmochim. Acta* **2011**, *75* (8), 2062−2071.
(76) Argyris, D.; Phan, A.; Striolo, A.; Ashby, P. D. Hydration structure at the α-Al2O3 (0001) surface: Insights from experimental atomic force spectroscopic data and atomistic molecular dynamics simulations. *J. Phys. Chem. C* **2013**, *117* (20), 10433−10444.
(77) Hu, X. L.; Michaelides, A. Water on the hydroxylated (0 0 1) surface of kaolinite: From monomer adsorption to a flat 2D wetting layer. *Surf. Sci.* **2008**, *602* (4), 960−974.
(78) Chen, J.; Min, F.-f.; Liu, L.-y.; Liu, C.-f. Mechanism research on surface hydration of kaolinite, insights from DFT and MD simulations. *Appl. Surf. Sci.* **2019**, *476*, 6−15.
(79) Argyris, D.; Cole, D. R.; Striolo, A. Hydration structure on crystalline silica substrates. *Langmuir* **2009**, *25* (14), 8025−8035.
(80) Phan, A.; Ho, T. A.; Cole, D.; Striolo, A. Molecular structure and dynamics in thin water films at metal oxide surfaces: magnesium, aluminum, and silicon oxide surfaces. *J. Phys. Chem. C* **2012**, *116* (30), 15962−15973.

https://doi.org/10.1021/acs.langmuir.1c02077
Langmuir 2022, 38, 914−926

(81) Liu, X.; Cheng, J.; Sprik, M.; Lu, X.; Wang, R. Understanding surface acidity of gibbsite with first principles molecular dynamics simulations. *Geochim. Cosmochim. Acta* **2013**, *120*, 487−495.
(82) Bickmore, B. R.; Tadanier, C. J.; Rosso, K. M.; Monn, W. D.; Eggett, D. L. Bond-valence methods for pKa prediction: critical reanalysis and a new approach. *Geochim. Cosmochim. Acta* **2004**, *68* (9), 2025−2042.
(83) Preocanin, T.; Abdelmonem, A.; Montavon, G.; Luetzenkirchen, J. Charging behavior of clays and clay minerals in aqueous electrolyte solutions—experimental methods for measuring the charge and interpreting the results. *Clays, Clay Minerals and Ceramic Materials Based on Clay Minerals*; InTech, 2016; pp 51−88.
(84) Pouvreau, M.; Greathouse, J. A.; Cygan, R. T.; Kalinichev, A. G. Structure of hydrated gibbsite and brucite edge surfaces: DFT results and further development of the clayFF classical force field with metal-O-H angle bending terms. *J. Phys. Chem. C* **2017**, *121* (27), 14757−14771.
(85) Teppen, B. J.; Rasmussen, K.; Bertsch, P. M.; Miller, D. M.; Schaefer, L. Molecular dynamics modeling of clay minerals. 1. Gibbsite, kaolinite, pyrophyllite, and beidellite. *J. Phys. Chem. B* **1997**, *101* (9), 1579−1587.
(86) Veilly, E.; Roques, J.; Jodin-Caumon, M.-C.; Humbert, B.; Drot, R.; Simoni, E. Uranyl interaction with the hydrated (001) basal face of gibbsite: A combined theoretical and spectroscopic study. *the journal of chemical physics* **2008**, *129* (24), 244704.
(87) Wang, J.; Kalinichev, A. G.; Kirkpatrick, R. J. Effects of substrate structure and composition on the structure, dynamics, and energetics of water at mineral surfaces: A molecular dynamics modeling study. *Geochimica et cosmochimica acta* **2006**, *70* (3), 562−582.
(88) Adler, J. J.; Rabinovich, Y. I.; Moudgil, B. M. Origins of the non-DLVO force between glass surfaces in aqueous solution. *J. Colloid Interface Sci.* **2001**, *237* (2), 249−258.
(89) Horn, R.; Smith, D.; Haller, W. Surface forces and viscosity of water measured between silica sheets. *Chem. Phys. Lett.* **1989**, *162* (4−5), 404−408.
(90) Grabbe, A.; Horn, R. G. Double-layer and hydration forces measured between silica sheets subjected to various surface treatments. *J. Colloid Interface Sci.* **1993**, *157* (2), 375−383.
(91) Chapel, J.-P. Electrolyte species dependent hydration forces between silica surfaces. *Langmuir* **1994**, *10* (11), 4237−4243.
(92) Vigil, G.; Xu, Z.; Steinberg, S.; Israelachvili, J. Interactions of silica surfaces. *J. Colloid Interface Sci.* **1994**, *165* (2), 367−385.
(93) Fielden, M. L.; Hayes, R. A.; Ralston, J. Oscillatory and ion-correlation forces observed in direct force measurements between silica surfaces in concentrated CaCl 2 solutions. *Phys. Chem. Chem. Phys.* **2000**, *2* (11), 2623−2628.
(94) Israelachvili, J.; Wennerström, H. Role of hydration and water structure in biological and colloidal interactions. *Nature* **1996**, *379* (6562), 219.
(95) Ducker, W. A.; Senden, T. J.; Pashley, R. M. Measurement of forces in liquids using a force microscope. *Langmuir* **1992**, *8* (7), 1831−1836.
(96) Ducker, W. A.; Senden, T. J.; Pashley, R. M. Direct measurement of colloidal forces using an atomic force microscope. *Nature* **1991**, *353* (6341), 239.
(97) Tuladhar, A.; Dewan, S.; Pezzotti, S.; Brigiano, F. S.; Creazzo, F.; Gaigeot, M.-P.; Borguet, E. Ions Tune Interfacial Water Structure and Modulate Hydrophobic Interactions at Silica Surfaces. *J. Am. Chem. Soc.* **2020**, *142* (15), 6991−7000.
(98) Pfeiffer-Laplaud, M.; Gaigeot, M.-P.; Sulpizi, M. p K a at Quartz/Electrolyte Interfaces. *journal of physical chemistry letters* **2016**, *7* (16), 3229−3234.
(99) Lowe, B.; Maekawa, Y.; Shibuta, Y.; Sakata, T.; Skylaris, C.-K.; Green, N. Dynamic behaviour of the silica-water-bio electrical double layer in the presence of a divalent electrolyte. *Phys. Chem. Chem. Phys.* **2017**, *19* (4), 2687−2701.
(100) Cimas, Á.; Tielens, F.; Sulpizi, M.; Gaigeot, M.-P.; Costa, D. The amorphous silica-liquid water interface studied by ab initio molecular dynamics (AIMD): local organization in global disorder. *J. Phys.: Condens. Matter* **2014**, *26* (24), 244106.
(101) Sakuma, H.; Kawamura, K. Structure and dynamics of water on Li+-, Na+-, K+-, Cs+-, H3O+-exchanged muscovite surfaces: A molecular dynamics study. *Geochim. Cosmochim. Acta* **2011**, *75* (1), 63−81.
(102) Dewan, S.; Yeganeh, M. S.; Borguet, E. Experimental correlation between interfacial water structure and mineral reactivity. *journal of physical chemistry letters* **2013**, *4* (11), 1977−1982.
(103) Schrader, A. M.; Monroe, J. I.; Sheil, R.; Dobbs, H. A.; Keller, T. J.; Li, Y.; Jain, S.; Shell, M. S.; Israelachvili, J. N.; Han, S. Surface chemical heterogeneity modulates silica surface hydration. *Proc. Natl. Acad. Sci. U. S. A.* **2018**, *115* (12), 2890−2895.
(104) Sivan, U. The inevitable accumulation of large ions and neutral molecules near hydrophobic surfaces and small ions near hydrophilic ones. *Curr. Opin. Colloid Interface Sci.* **2016**, *22*, 1−7.

https://doi.org/10.1021/acs.langmuir.1c02077
Langmuir 2022, 38, 914−926